Natural Frame Control of Single-Phase Cascaded H-Bridge Multilevel Converter Based on Fictive-Phases Construction

Daliang Yang, Ning Wu, Li Yin, and Ziguang Lu

***Abstract*—In this paper, a novel natural frame control is proposed for a single-phase cascaded H-bridge (CHB) multilevel converter. Natural frame control can acquire sinusoidal current waveform and achieve the balanced control of dc-link voltage without phase-locked loop or any coordinate transformation. Compared with conventional single-phase *dq* control, it only needs an imaginary voltage component without requiring an imaginary current component, which can eliminate additional current delay. Moreover, a new imaginary voltage construction method, referred to as fictive-phase construction (FPC), based on phase leading is presented. The delay time of FPC is only 1.67 ms theoretically under the condition of 50-Hz frequency, which is faster than the existing delay time of 5 or 3.33 ms. This effectively improves the real-time performance of the system when grid voltage fluctuates. Simulation and experimental results for a three-cell CHB converter validate the proposed control method.**

***Index Terms*—Cascaded H-bridge (CHB), fictive-phases construction (FPC), multilevel converter, natural frame control.**

Nomenclature

f	Signal frequency (in hertz).
f_s	Sampling frequency (in hertz).
δ	Phase difference between the two adjacent sampling points (in degrees).
N	Sampling points per signal cycle.
n	Data interval.
φ	Phase difference between the two sampling data (in degrees).
e_a, e_b, e_c	Instantaneous three-phase grid voltage. (in volts).
$e_a^\wedge$, $e_b^\wedge$, $e_c^\wedge$	Orthogonal components of the corresponding instantaneous three-phase grid voltage. (in volts).
e_s	Active voltage vector.
$e_s^\wedge$	Reactive voltage vector.
e_α, e_β	Components of e_s in stationary reference frame.
v_a, v_b, v_c	Active voltage unit vector.
w_a, w_b, w_c	Reactive voltage unit vector.
i_p^*, i_q^*	Active and reactive current references.
i_{pa}^*, i_{pb}^*, i_{pc}^*	Three-phase active current references.
i_{qa}^*, i_{qb}^*, i_{qc}^*	Three-phase reactive current references.
i_{sa}^*, $i^*{}_{sb}$, $i^*{}_{sa}$	Total three-phase current references.

Manuscript received April 10, 2017; revised July 8, 2017 and September 3, 2017; accepted September 21, 2017. Date of publication October 6, 2017; date of current version January 16, 2018. *(Corresponding author: Daliang Yang.)*

The authors are with the College of Electrical Engineering, Guangxi University, Nanning 530004, China (e-mail: yangdl@gxu.edu.cn; eewuning@mail.gxu.cn; 15521318432@163.com; luzg@gxu.edu.cn).

Color versions of one or more of the figures in this paper are available online at http://ieeexplore.ieee.org.

Digital Object Identifier 10.1109/TIE.2017.2760852

I. Introduction

In RECENT years, single-phase cascaded H-bridge (CHB) multilevel converters is one of the most popular multilevel topologies, due to its modular structure, lower switching frequency, simple layout, and small number of components, compared with other multilevel topologies [1], [2]. These advantages make the CHB converter the key element in the control structure of many medium- and high-power applications. It has been employed in solid-state transformers [3], [4], static synchronous compensators [5], [6], grid-connected photovoltaic (PV) systems [7]–[9], and active rectifier [10].

Since the CHB multilevel converters feature several dc-links (see Fig. 1), the general control scheme needs to fulfill a double task: ac-side sinusoidal current with a unity power factor, and balanced control of the dc-link voltage. During recent years, several strategies have been proposed, (e.g., passivity-based, predictive, and proportional-integral (PI)-based control schemes), in order to achieve current regulation and balance control of CHB converters [11]–[13].

Generally, synchronous frame control, also called *dq* control, and stationary frame control have been widely used for current control of single-phase or three-phase pulse width modulation (PWM) converters [14]–[17]. In *dq* control, ac variables are transformed to the equivalent dc quantities by coordinate transformation. Next, the PI controllers can be used to achieve zero steady state errors due to their dc infinite gain, which can make the system obtain fast response times and good stability [18]. In [19] and [20], a single-phase *dq* control method is presented for CHB converters. This scheme can acquire sinusoidal current waveform with a unity power factor and keep the dc-link voltage the same. In stationary frame control, including stationary reference frame control and conventional natural frame control, active and reactive current command are transformed to the ac current reference by coordinate transformation. The

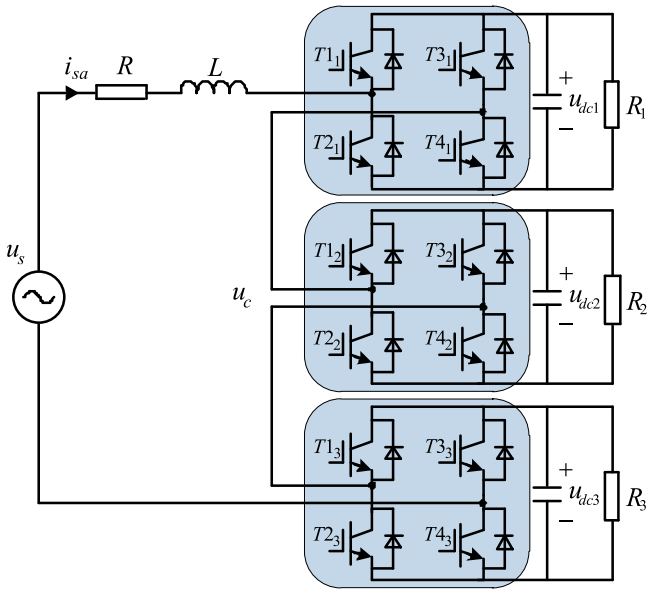

Fig. 1. Three-cell single-phase CHB converter.

proportional-resonant (PR) controllers can, then, be adopted to track ac reference signals with zero steady state error. The PR controllers provide an infinite gain at the concerned frequency to eliminate zero steady state error, which is basically equivalent (in view of the concerned frequency) to PI controllers in the *dq* frame [21]. In [22], the control idea based on the natural reference frame has been proposed for three-phase grid-tied converters. This method can achieve individual control for each grid current using PR controllers. However, all of the above-mentioned control schemes in synchronous or stationary frames are based on phase-locked loop (PLL) and coordination transformation. Usually, the PLL is used to obtain the grid voltage angle. The advantage is a better rejection of grid harmonics, but the algorithm will be more complex when grid voltage is unbalanced or fluctuated. Therefore, the computational complexity of PLL and multiple coordinate transformations increases the calculation burden of the embedded processor, such as the digital signal processor (DSP) and field-programmable gate array.

The *dq* control were originally introduced for three-phase systems, and then extended to single-phase applications. It cannot be directly applied to a stationary-to-rotating frame ($\alpha\beta$ to *dq*) transformation, as a single-phase system contains only one phase physical variable. The imaginary orthogonal signals, including voltage and current signal, in conventional methods are acquired by phase shifting the measured real signals using a 1/4 of the fundamental period. The conventional method tends to deteriorate the dynamic performance and can be oscillatory, because of a delay of 1/4 of the fundamental period [23]. Instead of time-delay methods, improved single-phase *dq* control methods have been proposed. The fictive-axis emulation method is proposed in [24], where the imaginary current is generated by virtually emulating the output filter inductor in the controller. Thus, its performance and response depends on the system parameters. In another approach, the novel orthogonal signal generation method employed active and reactive current command to estimate imaginary current signal [25]. Although this method offers a fast and robust *dq* current controller, the initial phase of the imaginary current is calculated by the arctangent function, which is limited for the value of the current reference.

With the rapid development of renewable energy resources (RES) such as solar and wind energy, a high penetration of PV and wind generation may significantly impact power systems, leading to increased fluctuation of grid frequency, and voltage amplitude [26], [27]. In the conventional imaginary voltage construction method of single-phase systems, the imaginary voltage was constructed by the phase-lagging measured voltage signal by 1/4 or 1/6 of the fundamental period [28], [29]. The delay time is 5 or 3.33 ms under the condition of 50-Hz frequency when voltage signal fluctuates. Unlike common imaginary voltage construction approaches based on phase lagging, a new method called the fictive-phase construction (FPC) is presented, further improving the real-time performance of the system due to the time delay of 1.67 ms.

In this paper, a novel natural frame control is proposed for single-phase CHB multilevel converters, by introducing an active voltage unit vector (AVUV) and reactive voltage unit vector (RVUV). In the proposed control methods, ac-side sinusoidal current with a unity power factor and balanced control of the dc-link voltage can be achieved without PLL or any coordination transformation. Compared with conventional single-phase *dq* control, natural frame control needs only the imaginary voltage component, not imaginary current component, which can eliminate additional current delay. Moreover, FPC was proposed to improve real-time performance when single-phase grid voltage fluctuates, such as voltage sag and voltage swell.

This paper is organized as follows. First, the principle of the FPC method and natural frame control is explained in Section II. Next, the simulation results are described in Section III. Section IV shows the experimental results that verify the proper operation of the CHB converter, and Section V concludes this paper.

II. Principle of Control Method

A. Topology of the CHB Multilevel Converter

Fig. 1 shows a three-cell H-bridge system connected in series, where u_s is the grid voltage, i_{sa} is the ac-side current, R is the input line resistance, L is the input inductor, and u_c is the ac-side voltages of the CHB converter. The u_{dc1}, u_{dc2}, and u_{dc3} are the c-side voltages across the capacitor of the H-bridge. R_1, R_2, and R_3 are pure resistive loads connected to dc-side of each cell.

B. Presentation of FPC Method

The conventional control scheme is unable be used directly, because the single-phase system contains only one phase physical variable. Normally, there are two approaches constructing imaginary multiphase systems. The first is to introduce a phase lagging of 90°, with respect to the fundamental frequency of the real signal, constructing the orthogonal $\alpha\beta$ frame [28]. This method is called the $\alpha\beta$ construction method. The second is as follows: $-u_c$ is obtained through a 60° delay of u_a; then u_b

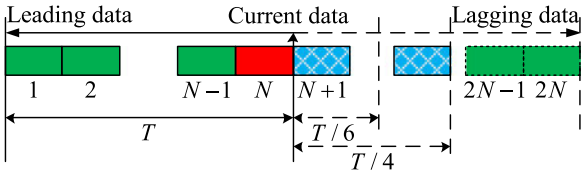

Fig. 2. Schematic diagram for sampling real-time data and lead-lag data

is calculated by $u_b = -u_a - u_c$ [29]. As a result, a symmetrical *abc* frame is built, which is called the *abc* construction method. With the increased penetration level of RES in power systems, the delay time of the conventional imaginary voltage construction method is 5 or 3.33 ms under the condition of 50-Hz frequency. Therefore, a new voltage construction approach is proposed in this paper, to improve the real-time performance when voltage fluctuated.

1) Principle of the New Algorithm: Let T represent a signal cycle time and N is the number of data samples per cycle. The relationship between the data- sampling time of the algorithm and the data of the leading and lagging time is shown in Fig. 2. Regarding the newest sampling data as the Nth sample, the previous historical data is recognized as the phase-leading data, and the phase-lagging data can only be obtained by the next moment or a longer time delay. Taking phase shifting 60° and 90° as an example, the delay time is 1/4 and 1/6 of the fundamental period, respectively. The imaginary signal data is not credible during this period, and this phenomenon is called "abnormal detection" [30]. From Fig. 2, it can be concluded that the constructed imaginary signal, whether using the phase-leading or phase-lagging data, always has an "abnormal detection" phenomenon. The delay time is equal to the phase difference between the imaginary signal and the actual detection signal. Therefore, the challenge is to reduce the phase difference between both sides rather than use leading or lagging data. Unlike conventional methods based on phase lagging, the new FPC method is grounded on the idea of phase leading.

2) Selection of Sampling Frequency: In order to construct the imaginary three-phase system accurately by FPC, how to select sampling frequency is described below.

Let f represent the signal frequency and f_s is the sampling frequency. The phase difference δ between the two adjacent sampling points is

$$\delta = \frac{f \times 360}{f_s}. \tag{1}$$

Let N represent the sampling points per signal cycle, which is $N = f_s/f$. The above equation can be written as

$$\delta = \frac{360}{N}. \tag{2}$$

If the angle difference between the two sampling data is φ, the data interval n in the sampling data sequence should be

$$n = \frac{\varphi}{\delta} = \varphi\frac{N}{360}. \tag{3}$$

The results of the above formula may appear decimal, and it is impossible to appear decimal in the actual sampling data. For this reason, the corresponding measures should be considered, to ensure that n is an integer. For example, the angle difference between the two sampling data is 30°, where the corresponding data interval n is shown in Table I when different a sampling frequency is selected. It can be seen from Table I that n is an integer when the sampling frequency is 9 or 7.2 kHz, while n is decimal when the sampling frequency is 12.8 or 10 kHz, which causes quantization error. The data that are 30° leading the current sampling data are found from the known sampling data, and are based on the data interval n between two sampling data. This is a factor when the sampling frequency is chosen.

TABLE I
DATA TABLE OF DIFFERENT SAMPLING FREQUENCIES

f_s	N	δ	Interval n of 30°
12.8 kHz	256	1.4063°	21.33
10 kHz	200	1.8°	16.67
9 kHz	180	2°	15
7.2 kHz	144	2.5°	12

C. Principle of Natural Frame Control

In a balanced, sinusoidal, and three-phase circuit, active and reactive powers are the most important information that represents the main characteristics of the system. Applying this information, three-phase instantaneous voltage can be directly transformed into active and reactive voltage, achieving the independent control of active and reactive current, respectively.

The instantaneous active power p and reactive power q in the natural frame can be described as

$$\begin{bmatrix} p \\ q \end{bmatrix} = \begin{bmatrix} e_a & e_b & e_c \\ e_a^{\wedge} & e_b^{\wedge} & e_c^{\wedge} \end{bmatrix} \begin{bmatrix} i_a \\ i_b \\ i_c \end{bmatrix} \tag{4}$$

where i_a, i_b, and i_c represent the instantaneous three-phase grid current, e_a, e_b, and e_c represent the instantaneous three-phase grid voltage, and $e_a^{\wedge}$, $e_b^{\wedge}$, and $e_c^{\wedge}$ represent orthogonal components of the corresponding instantaneous three-phase grid voltage given by following equation:

$$\begin{bmatrix} e_a^{\wedge} \\ e_b^{\wedge} \\ e_c^{\wedge} \end{bmatrix} = \frac{1}{\sqrt{3}} \begin{bmatrix} e_b - e_c \\ e_c - e_a \\ e_a - e_b \end{bmatrix}. \tag{5}$$

Define $e_s = (e_a, e_b, e_c)^T$ as the active voltage vector and $e_s^{\wedge} = (e_a^{\wedge}, e_b^{\wedge}, e_c^{\wedge})$ as the reactive voltage vector. The active voltage vector is equal to the amplitude of the reactive voltage vector, and is 90° lagging with the reactive voltage vector. The relationship between the two kinds of vectors is shown in the Fig. 3.

Considering the symmetry of a balanced three-phase system, the amplitude of the active voltage vector $e_s = (e_a, e_b, e_c)^T$ is a constant which can be described as

$$e_s = \sqrt{e_\alpha{}^2 + e_\beta{}^2} \tag{6}$$

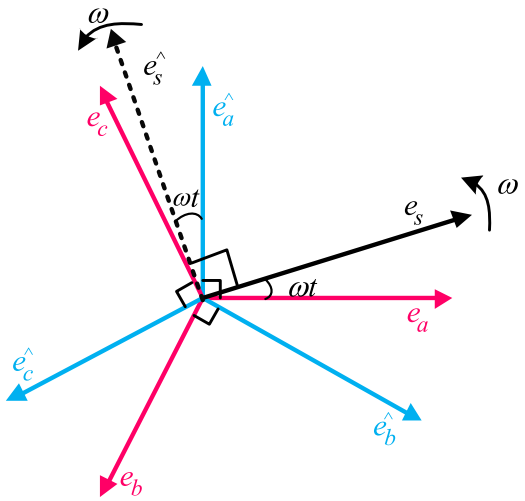

Fig. 3. Relationship between active voltage vector and reactive voltage vector in natural frame.

where e_α and e_β represent the components of e_s in the stationary reference frame ($\alpha\beta$ frame).

According to the Clarke transformation

$$\begin{bmatrix} e_\alpha \\ e_\beta \end{bmatrix} = \frac{2}{3}\begin{bmatrix} 1 & -\frac{1}{2} & -\frac{1}{2} \\ 0 & \frac{\sqrt{3}}{2} & -\frac{\sqrt{3}}{2} \end{bmatrix}\begin{bmatrix} e_a \\ e_b \\ e_c \end{bmatrix}. \tag{7}$$

By substituting e_α and e_β from (7) into (6), the following equation is deduced:

$$e_s = \sqrt{\frac{2}{3}\left({e_a}^2 + {e_b}^2 + {e_c}^2\right)}. \tag{8}$$

The AVUV is derived as follows:

$$\begin{bmatrix} v_a \\ v_b \\ v_c \end{bmatrix} = \frac{1}{e_s}\begin{bmatrix} e_a \\ e_b \\ e_c \end{bmatrix}. \tag{9}$$

The RVUV is derived as follows:

$$\begin{bmatrix} w_a \\ w_b \\ w_c \end{bmatrix} = \frac{1}{\hat{e_s}}\begin{bmatrix} \hat{e_a} \\ \hat{e_b} \\ \hat{e_c} \end{bmatrix}. \tag{10}$$

According to the relationship between the active voltage vector and the reactive voltage vector, the RVUV can be expressed by the AVUV, written as the following equation:

$$\begin{bmatrix} w_a \\ w_b \\ w_c \end{bmatrix} = \frac{1}{\sqrt{3}}\begin{bmatrix} 0 & -1 & 1 \\ 1 & 0 & -1 \\ -1 & 1 & 0 \end{bmatrix}\begin{bmatrix} v_a \\ v_b \\ v_c \end{bmatrix}. \tag{11}$$

Define i_p^* as the active current reference. Multiplication of AVUV (v_a, v_b, v_c) with i_p^* yields the active component of the ac reference currents (i_{pa}^*, i_{pb}^*, i_{pc}^*) given as follows:

$$\begin{bmatrix} i_{pa}^* \\ i_{pb}^* \\ i_{pc}^* \end{bmatrix} = i_p^*\begin{bmatrix} v_a \\ v_b \\ v_c \end{bmatrix}. \tag{12}$$

Define i_q^* as the reactive current reference. Multiplication of RVUV (w_a, w_b, w_c) with i_q^* produces the reactive component of the ac reference currents (i_{qa}^*, i_{qb}^*, i_{qc}^*), given as follows:

$$\begin{bmatrix} i_{qa}^* \\ i_{qb}^* \\ i_{qc}^* \end{bmatrix} = i_q^*\begin{bmatrix} w_a \\ w_b \\ w_c \end{bmatrix}. \tag{13}$$

The total reference currents are given as follows, using (12) and (13). From (14), the total reference current is the sum of the active and reactive components of the reference currents

$$\begin{bmatrix} i_{sa}^* \\ i_{sb}^* \\ i_{sc}^* \end{bmatrix} = \begin{bmatrix} i_{pa}^* \\ i_{pb}^* \\ i_{pc}^* \end{bmatrix} + \begin{bmatrix} i_{qa}^* \\ i_{qb}^* \\ i_{qc}^* \end{bmatrix}. \tag{14}$$

Note that the CHB converter is applied in the single-phase system, using one phase current reference as current reference.

D. Natural Frame Control of the CHB Converter

The entire control diagram of natural frame control is shown in Fig. 4, where the control system is formed as a double closed-loop control structure by the outer voltage loop and the inner current loop. The three-phase system is constructed by the FPC method. The AVUV (v_a, v_b, v_c) and RVUV (w_a, w_b, w_c) are calculated using (8)–(11). The outer voltage loop regulates the total dc voltage and output active current reference i_p^* by a PI controller. The reactive current reference i_q^* is directly given. A voltage balance control module is used, in order to obtain the current reference of each H-bridge. Errors between the measured current i_{sa} and current reference, i_{sa1}^*, i_{sa2}^*, and i_{sa3}^*, are input to the PR regulators that can track ac reference signals with zero steady state error, generating modulation voltage signals u_{sa1}^*, u_{sa2}^*, and u_{sa3}^* for each H-bridge. To modulate the voltage signals u_{sa1}^*, u_{sa2}^*, and u_{sa3}^*, a carrier phase-shifted PWM (CPS-PWM) technology has been adopted. Meanwhile, the q-axis current references i_q^* are zero, which means the unit power factor can be achieved.

The voltage balance control module adjusts the current reference i_{sa1}^*, i_{sa2}^*, and i_{sa3}^* individually to achieve different real power distributions of the H-bridges. Fig. 5 illustrates the proposed voltage balance control module. In Fig. 5, i_p^* is calculated by the outer voltage loop. The individual dc-link voltages of three H-bridges, u_{dc1}, u_{dc2}, and u_{dc3}, are compared with the same dc-link voltage reference u_{ref} to generate p-axis compensation $\Delta p1$, $\Delta p2$, and $\Delta p3$ by a PI regulator. Next, $\Delta p1$, $\Delta p2$, and $\Delta p3$ are added to i_p^* to obtain the three p-axis references i_{p1}^*, i_{p2}^*, and i_{p3}^*. Current references i_{sa1}^*, i_{sa2}^*, and i_{sa3}^* for each H-bridge are calculated according to (12)–(14).

III. Simulation Results

To verify the proposed ideas, the simulation of the proposed methods is first conducted in the Simulink/MATLAB R2015a software environment.

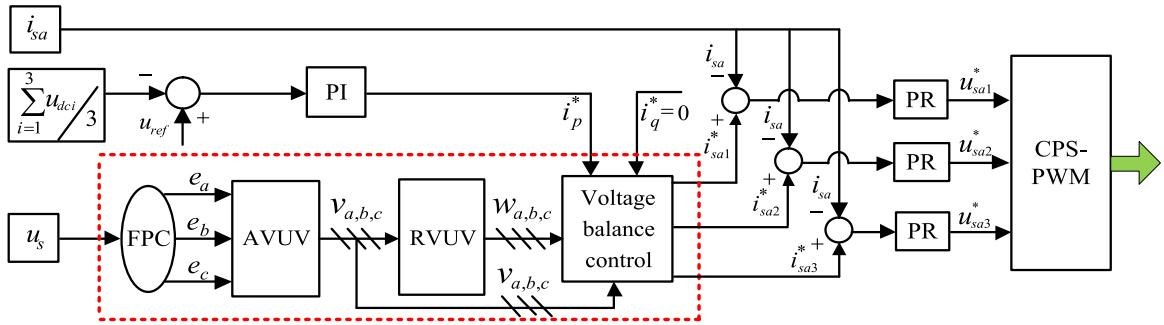

Fig. 4. Natural frame control of CHB converter.

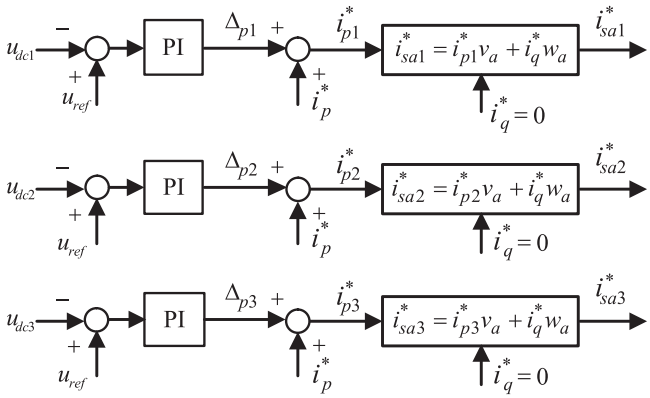

Fig. 5. Voltage balance control module.

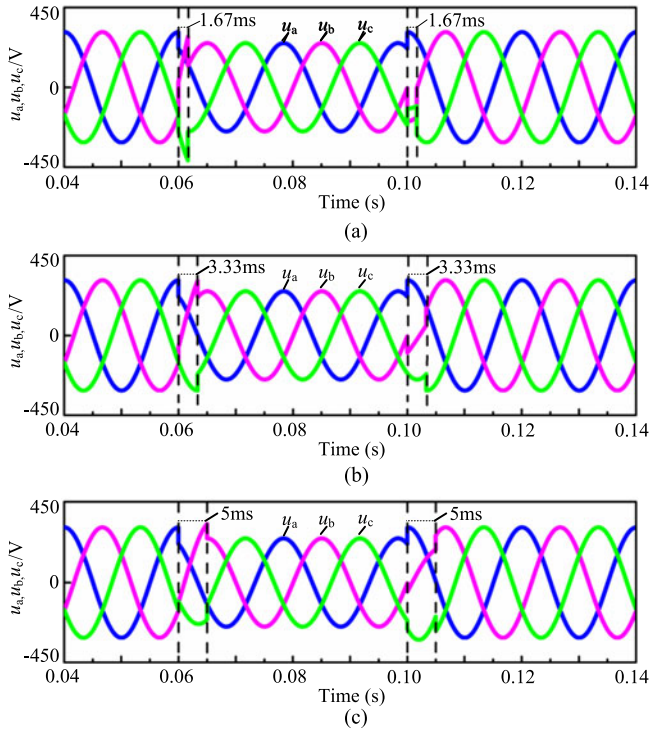

Fig. 6. Imaginary voltage construction results for 20% voltage sag and $\pi/6$ angle-shift. (a) FPC method. (b) *abc* construction method [29]. (c) $\alpha\beta$ construction method [28].

A. FPC Simulation

In order to determine if the proposed method is more suitable to create the imaginary voltage signal, it was compared with methods currently used. Assume that the measured single-phase voltage signal u_a is expressed as

$$u_a = \begin{cases} 220\sqrt{2}\cos(314t), & t \le 0.06 \text{ s or } t > 0.10 \text{ s} \\ 176\sqrt{2}\cos\left(314t + \frac{\pi}{6}\right), & 0.06 \text{ s} \le t \le 0.10 \text{ s}. \end{cases}$$

The voltage signal u_a experienced a 20% amplitude dip and $\pi/6$ phase jump during 0.06–0.10 s, where the duration is two fundamental periods. The start and end time of voltage sag is instantaneous.

The simulation results of different imaginary voltage construction methods are shown in Fig. 6 when reference voltage signal fluctuates. It can be observed from Fig. 6 that the variation of voltage amplitude is only 20%, but all methods can detect the voltage fluctuation effectively, constructing other two-phase voltage signals correctly. From the comparative simulation results it can be concluded that the delay time of the FPC method is 1.67 ms, and the delay time of the *abc* construction method is 3.33 ms, while the delay time of the $\alpha\beta$ construction method is 5 ms. The simulation results are consistent with the theoretical analysis.

B. Natural Frame Control Simulation

The CHB converter that was illustrated in Fig. 1 was used in the simulation and the main parameters for the system are shown in Table II. Fig. 7 shows the grid current and grid voltage waveform in steady state when a 15-Ω resistor is connected in each dc-link. Fig. 8 shows the seven-level staircase voltage generated on the ac-side of the three-cell CHB converter. The

TABLE II
SIMULATION PARAMETERS OF THE SYSTEM

Parameter	Value
Grid voltage *rms* value (u_s)	220 V
Grid frequency (f_g)	50 Hz
Input inductance (L)	3.0 mH
DC-link total voltage (U_{dc})	400 V
DC-link capacitance (C)	10^4 μF
DC-link load resistance	15 Ω
Voltage controller parameter (P,I)	0.1,10
Current controller parameter (P, R, w_c)	0.5, 100, 6.28

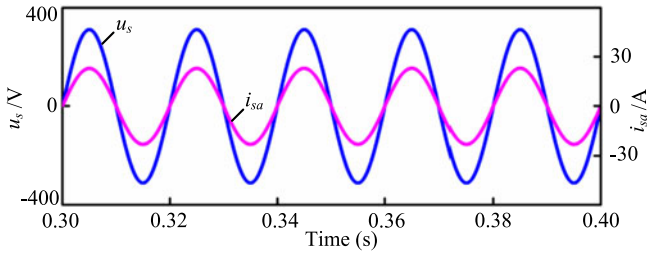

Fig. 7. Grid voltage and grid current.

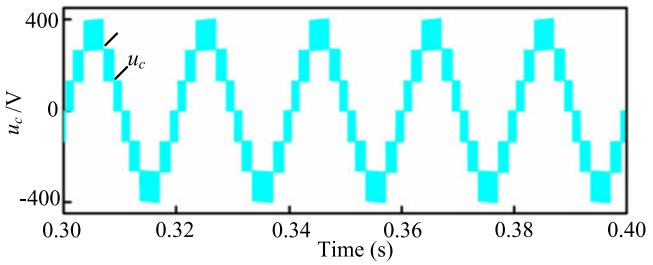

Fig. 8. Seven-level voltage waveform on ac side of three-cell CHB converter.

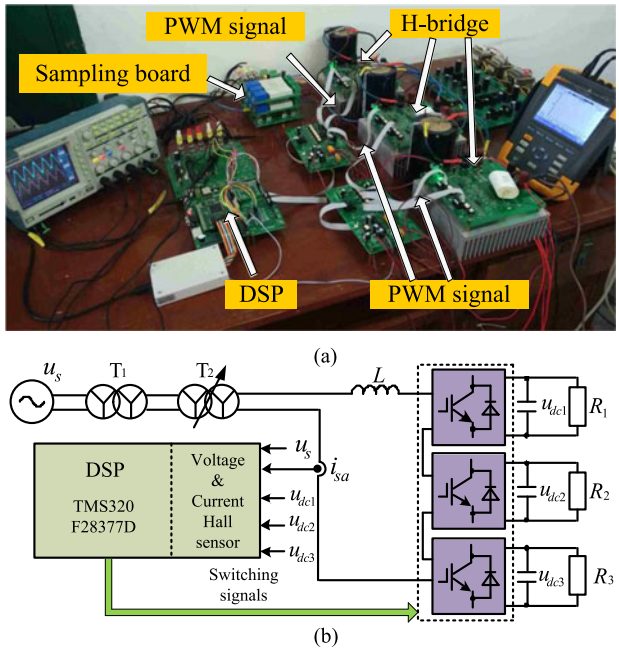

Fig. 9. Three-cell CHB converter experimental setup. (a) Picture of the experimental setup. (b) System diagram.

natural frame control without PLL or coordinate transformation can also generate high-quality current waveform and achieve the unity power factor, compared with Fig. 8 in [19] that uses single-phase *dq* control.

IV. Experimental Results

A. Experimental Prototype

A 1-kVA, down-scaled, experimental prototype of the single-phase CHB converter shown in Fig. 1 was created to verify the proposed control method. Fig. 9(a) depicts the experimental setup, where the H-bridge is designed by insulated gate bipolar transistor. Fig. 9(b) shows the block diagram of the experimental setup. The proposed algorithm was implemented by CPU1 of the TMS320F28377D 32-bit, floating-point DSP. The CPS-PWM technology used programmable, phase-control, and enhanced PWM modules. The grid voltage, grid current, and dc voltages were measured via built-in, 16-bit ADC and outer high-performance hall sensors. The system adopted switching frequencies equal to the sampling frequency of 9 kHz, which can ensure the data interval n is an integer. The dead time of the PWM signals is 5 μs. The converter is connected to the utility grid u_s through a coupling transformer T_1 and a voltage regulator T_2, which can ensure experimental equipment safety. Secondary-side voltage of the regulator T2 is set to 100 V (rms), while the dc-side capacitor voltage references are set to 50 V in each H-bridge. The other experimental parameters are the same as simulation parameters.

B. Experimental Results

Fig. 10 illustrates the experimental results using the control diagram shown in Fig. 4. The grid current is nearly sinusoidal

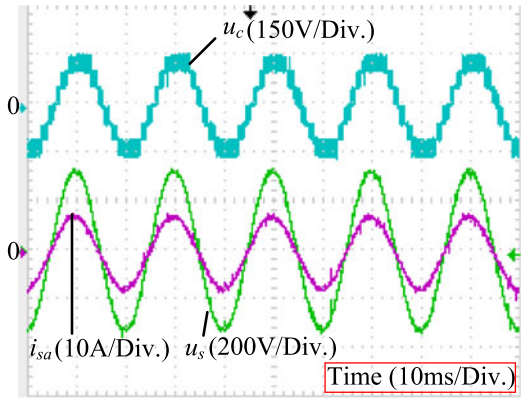

Fig. 10. Experimental grid currents in steady state.

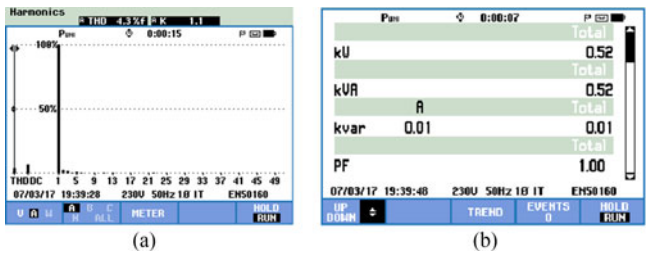

Fig. 11. THD of grid current and power factor in steady state.

shape with low harmonic distortion. The total harmonic distortion (THD) of the grid current shown in Fig. 10 is 4.3%, as shown in Fig. 11(a). This is less than 5% and meets power quality standards, like IEEE 1547 in the U.S and IEC61727 in Europe. From Fig. 11(b), it can be noticed that the unit power

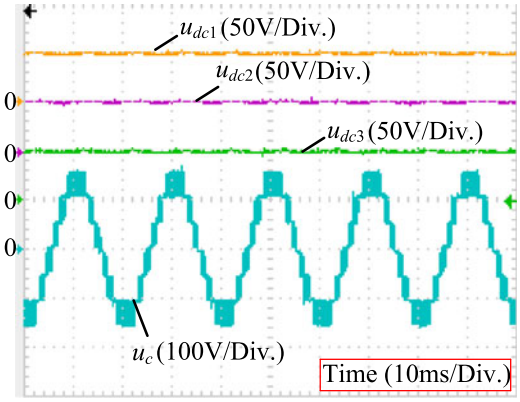

Fig. 12. Experimental dc-link voltage of H-bridge in steady state.

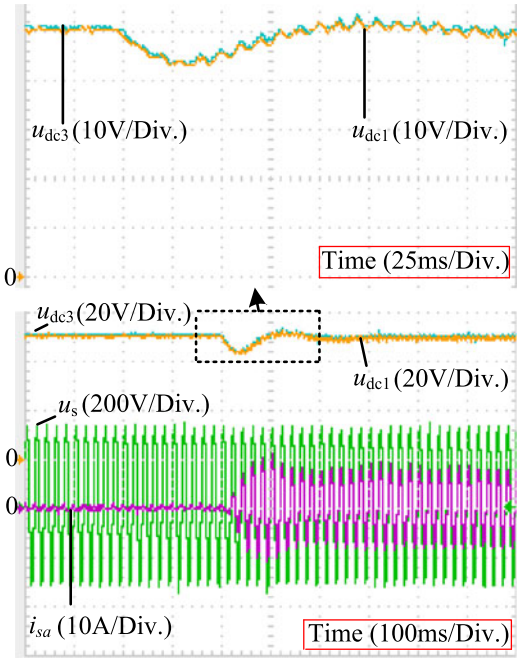

Fig. 13. Experimental dc-link voltage of H-bridge in transient state.

factor can be achieved by natural frame control. Fig. 12 shows the seven-level voltage produced on the ac-side of the CHB converter and the dc-link capacitor voltage references are achieved in each H-bridge. Fig. 13 shows the transient results when the load is applied in each H-bridge. The drop voltage of the dc-link is 14% of the voltage reference, and the transient time is approximately four grid cycles. The DSP clock frequency is set to 200 MHz and the total execution time of the proposed method is approximately 5.77 μs, which is very fast and suitable for implementation in embedded processors.

C. Comparison With Single-Phase dq Control

To verify the control of the P&Q axes efficiently of the natural frame control, a step current reference change with natural frame control and conventional single-phase dq control was completed. For fairness of the comparison, the zero-crossing detection of post-processing blocks on the TMS320F28377D

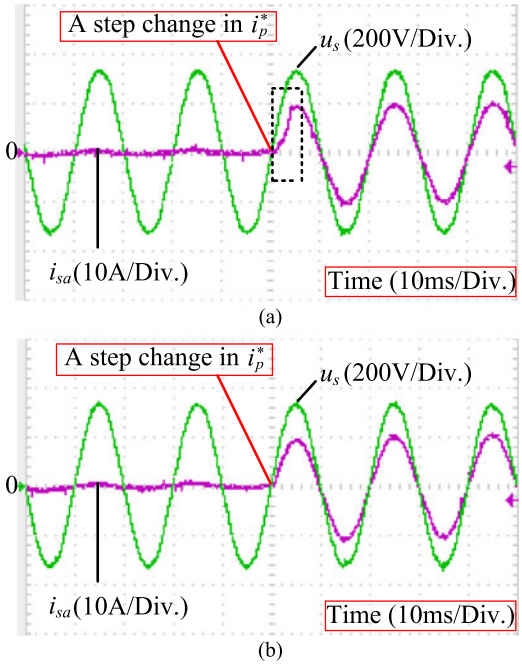

Fig. 14. Step current reference change of rectifying mode. (a) Conventional single-phase dq control. (b) Natural frame control.

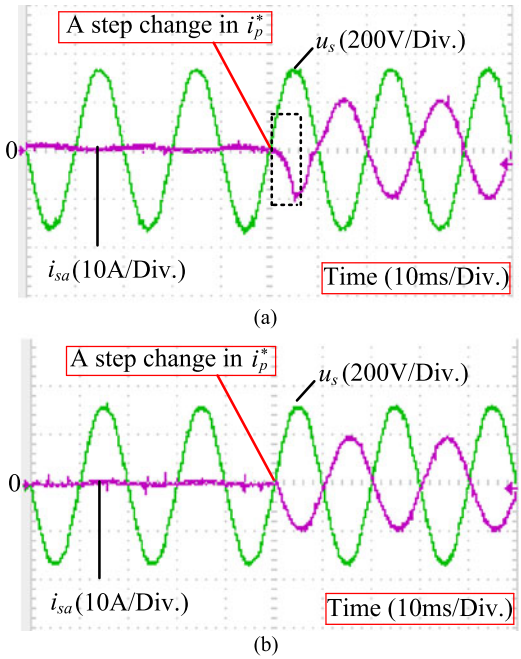

Fig. 15. Step current reference change of inverting mode. (a) Conventional single-phase dq control. (b) Natural frame control.

DSP was used to trigger step-change signals. Both i_p^* and i_q^* are stepped from 0 to 10 A or 0 to–10 A. The capacitor and resistor that connected to each dc-side of the H-bridge are substituted to the dc source at this moment.

Figs. 14–17 illustrate the dynamic performance with step current change in i_p^* and i_q^*. As observed in these figures, natural frame control makes system responses rapid, and can exactly track the new current reference within 1 ms, achieving P&Q axes

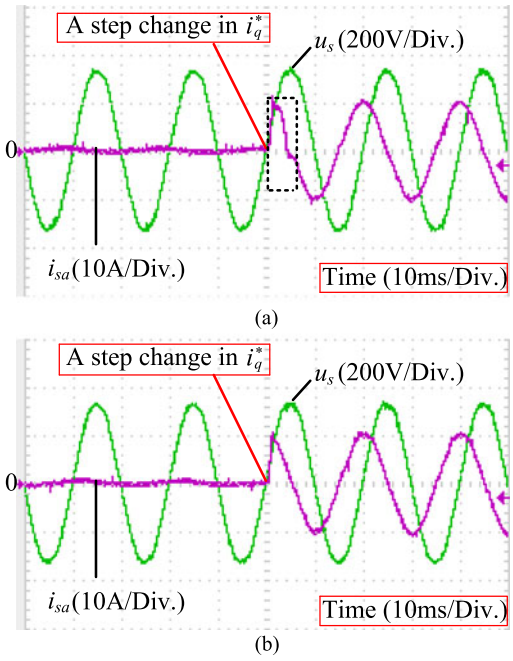

Fig. 16. Step current reference change of capacitive mode. (a) Conventional single-phase dq control. (b) Natural frame control.

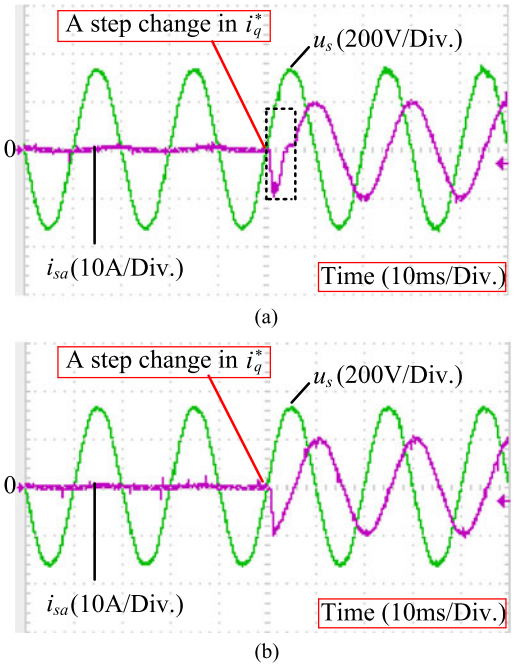

Fig. 17. Step current reference change of inductive mode. (a) Conventional single-phase dq control. (b) Natural frame control.

control, separately. Utilization of the single-phase *dq* control in this system, however, generates sustained distortion over 5 ms in grid-connected currents with step change. The reason is that the imaginary orthogonal current signal has to be created by a delay of 1/4 of the fundamental period in conventional single-phase *dq* control. The structure and performance comparison of natural frame control and conventional single-phase *dq* control is shown in Table III, according to the experimental tests.

TABLE III
STRUCTURE AND PERFORMANCE COMPARISON OF TWO METHODS BASED ON THE EXPERIMENTAL TESTS

Structure & Performance	Conventional Single-Phase *dq* Control	Natural Frame Control
Imaginary voltage component	Need	Need
Imaginary current component	Need	No
PLL	Need	No
Coordinate transformation	Need	No
Response of step current reference change	Slow	Fast
Total execution time	7.28 μs	5.77 μs

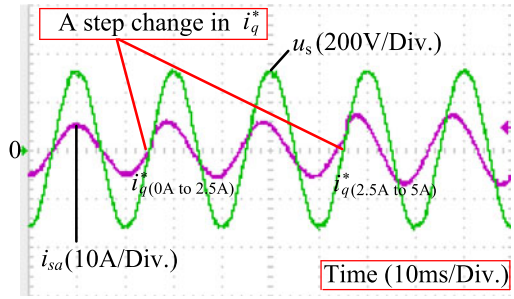

Fig. 18. Step current reference change in stepwise manner.

In order to further verify that natural frame control properly follows the current references, a dynamic test was performed. As can be seen in Fig. 18, the grid voltage u_s is in phase with grid current i_s when i_p^* is 5 A and i_q^* is 0 A initially. The value of i_q^* is stepped from 0 to 2.5 A. After 40 ms, i_q^* is stepped from 2.5 to 5 A. Along with the current reference changes, the phase difference between u_s and i_s has the corresponding change. The obtained results confirm the correct operation of natural frame control during current reference change.

D. Voltage Balance Control Based on Natural Frame Control

One of the main disadvantages of the CHB converter is the voltage unbalance of the dc-link due to the converter switching loss, time delay of the gate pulse, and H-bridge real power differences. In order to verify the voltage balance control, the load resistors R_1, R_2, and R_3 connected to the three dc-links u_{dc1}, u_{dc2}, and u_{dc3} are changed to create the load differences. In this experiment, the load resistor R_3 changes from 15 to 10 Ω, while R_1 and R_2 maintain as 15 Ω. Fig. 19 illustrates the three dc-link voltages without the voltage balance control. The three dc-link voltages are all regulated at 50 V when the loads are the same. However, after the loads change, the dc-link voltages become approximately 55, 55, and 40 V, respectively. The H-bridge with a larger load resister has a higher dc-link voltage (u_{dc1} and u_{dc2} in Fig. 19). Fig. 20 shows the three dc-link voltages with voltage balance control. The balance controller regulates the dc-link voltage when there is a load change. The dc-link voltages have a transit time of approximately five cycles, then settle down to be the same voltage. The experiment verifies the

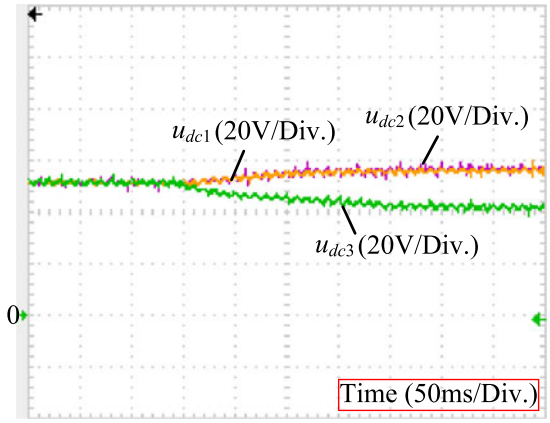

Fig. 19. DC-link voltages without voltage balanced control.

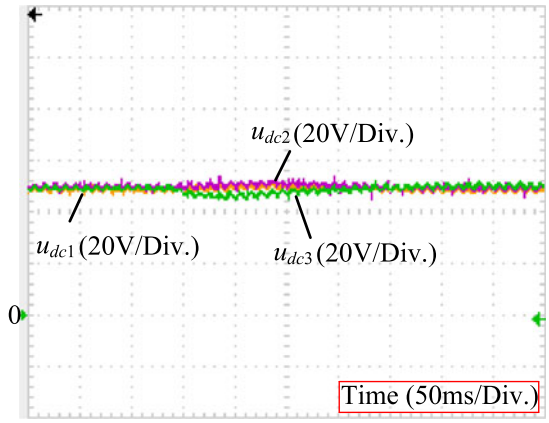

Fig. 20. DC-link voltages with voltage balanced control.

effectiveness of the natural frame control with voltage balance control.

V. Conclusion

In this paper, a novel natural frame control based on FPC for single-phase CHB multilevel converter has been proposed. The natural frame control can fulfill a double task: ac-side sinusoidal current with a unity power factor and balanced control of the dc-link voltage without PLL or any coordination transformation. Moreover, compared with single-phase *dq* control, natural frame control needs only the imaginary voltage component, not imaginary current component, which can eliminate additional current delay. The proposed FPC method not only creates a "symmetrical" and "stable" three-phase system, but also further improves the real-time performance of the system due to the 1.67 ms delay time. Simulation and experimental results for a three-cell H-bridge system have shown that the proposed natural frame control and FPC method operate together to achieve a sinusoidal current, unity power factor, and dc-link voltage balance. Natural frame control can apply to other PWM converters because of the simple structure and easy implementation. Due to the very short delay time of the FPC method, it is especially recommended for voltage sag detection.

References

[1] J. Rodriguez *et al.*, "Multilevel converters: An enabling technology for high-power applications," *Proc. IEEE*, vol. 97, no. 11, pp. 1786–1817, Nov. 2009.
[2] S. Kouro *et al.*, "Recent advances and industrial applications of multilevel converters," *IEEE Trans. Power Electron.*, vol. 57, no. 8, pp. 2553–2580, Aug. 2010
[3] T. Zhao, G. Wang, S. Bhattacharya, and A. Q. Huang, "Voltage and power balance control for a cascaded H-bridge converter-based solid-state transformer," *IEEE Trans. Power Electron.*, vol. 28, no. 4, pp. 1523–1532, Apr. 2013.
[4] X. She, X. Yu, F. Wang, and A. Q. Huang, "Design and demonstration of a 3.6-kV 120-V/10-kVA solid-state transformer for smart grid application," *IEEE Trans. Power Electron.*, vol. 29, no. 8, pp. 3982–3996, Aug. 2014.
[5] G. Farivar, B. Hredzak, and V. G Agelidis, "Decoupled control system for cascaded H-bridge multilevel converter based STATCOM," *IEEE Trans. Ind. Electron.*, vol. 63, no. 1, pp. 322–331, Jan. 2016.
[6] G. Farivar *et al.*, "Passive reactor compensated cascaded H-bridge multilevel LC-StatCom," *IEEE Trans. Ind. Electron.*, vol. 32, no. 11, pp. 8338–8348, Nov. 2017.
[7] E. Villanueva, P. Correa, J. Rodriguez, and M. Pacas, "Control of a single-phase cascaded H-bridge multilevel inverter for grid-connected photovoltaic systems," *IEEE Trans. Ind. Electron.*, vol. 56, no. 11, pp. 4399–4406, Nov. 2009.
[8] J. Chavarria, D. Biel, F. Guinjoan, C. Meza, and J. Negroni, "Energy balance control of PV cascaded multilevel grid-connected inverters for phase-shifted and level-shifted pulse-width modulations," *IEEE Trans. Ind. Electron.*, vol. 60, no. 1, pp. 98–111, Jan. 2013.
[9] G. Farivar, B. Hredzak, and V. G. Agelidis, "A DC-side sensorless cascaded H-bridge multilevel converter-based photovoltaic system," *IEEE Trans. Ind. Electron.*, vol. 64, no. 7, pp. 4233–4241, Jul. 2016.
[10] P. Karamanakos, K. Pavlou, and S. Manias, "An enumeration-based model predictive control strategy for the cascaded H-bridge multilevel rectifier," *IEEE Trans. Ind. Electron.*, vol. 61, no. 7, pp. 3480–3489, Jul. 2014.
[11] A. D. Aquila, M. Liserre, V. G. Monopoli, and P. Rotondo, "An energy based control for an *n*-H-bridges multilevel active rectifier," *IEEE Trans. Ind. Electron.*, vol. 52, no. 3, pp. 670–678, Jun. 2005.
[12] P. Zanchetta, D. B. Gerry, V. G. Monopoli, J. C. Clare, and P. W. Wheeler, "Predictive current control for multilevel active rectifiers with reduced switching frequency," *IEEE Trans. Ind. Electron.*, vol. 55, no. 1, pp. 163–172, Jan. 2008.
[13] A. Dell'Aquila, M. Liserre, V. Monopoli, and P. Rotondo, "Overview of pi-based solutions for the control of DC buses of a single-phase H-bridge multilevel active rectifier," *IEEE Trans. Ind. Appl.*, vol. 44, no. 3, pp. 857–866, May/Jun. 2008.
[14] D. N. Zmood and D. G. Holmes, "Stationary frame current regulation of PWM inverters with zero steady-state error," *IEEE Trans. Power Electron.*, vol. 18, no. 3, pp. 814–822, May 2003.
[15] R. Teodorescu, F. Blaabjerg, M. Liserre, and P. C. Loh, "Proportional–resonant controllers and filters for grid-connected voltage-source converters," *Proc. Inst. Elect. Eng.*, vol. 153, no. 5, pp. 750–762, Sep. 2006.
[16] Y. Gu, Y. Wang, X. Xiang, W. Li, and X. He, "Improved virtual vector control of single-phase inverter based on unified model," *IEEE Trans. Energy Convers.*, vol. 29, no. 3, pp. 611–618, Sep. 2014.
[17] B. Parkhideh and S. Bhattacharya, "Vector-controlled voltage-source converter-based transmission under grid disturbances," *IEEE Trans. Power Electron.*, vol. 28, no. 2, pp. 661–672, Feb. 2013.
[18] M. Monfared, S. Golestan, and J. M. Guerrero, "Analysis, design, and experimental verification of a synchronous reference frame voltage control for single-phase inverters," *IEEE Trans. Ind. Electron.*, vol. 61, no. 1, pp. 258–269, Jan. 2014.
[19] J. Shi, W. Gou, H. Yuan, T. Zhao, and A. Q. Huang, "Research on voltage and power balance control for cascaded modular solid-state transformer," *IEEE Trans. Power Electron.*, vol. 26, no. 4, pp. 1154–1166, Apr. 2011.
[20] X. She, A. Q. Huang, and G. Wang, "3-D space modulation with voltage balancing capability for a cascaded seven-level converter in a solid-state transformer," *IEEE Trans. Power Electron.*, vol. 26, no. 12, pp. 3778–3789, Dec. 2011.
[21] C. Zou, B. Liu, S. Duan, and R. Li, "Stationary frame equivalent model of proportional-integral controller in dq synchronous frame," *IEEE Trans. Power Electron.*, vol. 29, no. 9, pp. 4461–4465, Sep. 2014.
[22] F. Blaabjerg *et al.*, "Overview of control and grid synchronization for distributed power generation systems," *IEEE Trans. Ind. Electron.*, vol. 53, no. 5, pp. 1398–1409, Oct. 2006.

[23] S. Somkun and V. Chunkag, "Unified unbalanced synchronous reference frame current control for single-phase grid-connected voltage source converters," *IEEE Trans. Ind. Electron.*, vol. 63, no. 9, pp. 5425–5436, Sep. 2016.
[24] B. Bahrani, A. Rufer, S. Kenzelmann, and L. A. C. Lopes, "Vector control of single-phase voltage-source converters based on fictive-axis emulation," *IEEE Trans. Ind. Appl.*, vol. 47, no. 2, pp. 831–840, Mar./Apr. 2011.
[25] M. Ebrahimi, S. Khajehoddin, and M. Karimi Ghartemani, "Fast and robust single-phase dq current controller for smart inverter applications," *IEEE Trans. Power Electron.*, vol. 31, no. 5, pp. 3968–3976, May 2016.
[26] R. Yan and T. K. Saha, "Investigation of voltage stability for residential customers due to high photovoltaic penetrations," *IEEE Trans. Power Syst.*, vol. 27, no. 2, pp. 651–662, May 2012.
[27] J. I. Y. Ota, T. Sato, and H. Akagi, "Enhancement of performance, availability, and flexibility of a battery energy storage system based on a modular multilevel cascaded converter (MMCC-SSBC)," *IEEE Trans. Power Electron.*, vol. 31, no. 4, pp. 2791–2799, Apr. 2016.
[28] S. M. Silva, B. M. Lopes, B. J. C. Filho, R. P. Campana, and W. C. Bosventura, "Performance evaluation of PLL algorithms for single phase grid-connected systems," in *Proc. 39th Int. Conf. IEEE Ind. Appl.*, Oct. 2004, vol. 4, pp. 2259–2263.
[29] X. Xiangning, X. Yonghai, and L. Lianguang, "Simulation and analysis of voltage sag mitigation using active series voltage injection," in *Proc. Int. Conf. Power System Technol.*, 2000, pp. 1317–132.
[30] G. Chen, L. Zhang, R. Wang, L. Zhang, and X. Cai, "A novel SPLL and voltage sag detection based on LES filters and improved instantaneous symmetrical components method," *IEEE Trans. Power Electron.*, vol. 30, no. 3, pp. 1177–1188, Mar. 2015.

Daliang Yang received the B.S. degree from the Jilin University of Technology, Changchun, China, in 1998, and the M.S. degree from the University of Electronic Science and Technology of China, Chengdu, China, in 2003. He received the Ph.D. degree in electrical engineering from the Guangxi University, Nanning, China, in 2014, all in electrical engineering.

His research interests include pulse width modulation converter control, power electronic transformer, power quality, and application of power electronics.

Ning Wu was born in China in 1991. He received the B.S. degree in electrical engineering and automation from Tianjin Chengjian University, Tianjin, China, in 2015. He is currently working toward the M.S. degree in electrical engineering at the College of Electrical Engineering, Guangxi University, Nanning, China.

His research interests include digital signal processor controller and topology for cascaded H-bridge multilevel converter, and neutral point clamped converter.

Li Yin was born in 1994. He received the B.S. degree in electrical engineering and automation from Guangzhou University, Guangzhou, China, in July 2016. He is currently working toward the M.S. degree in electrical engineering at the College of Electrical Engineering, Guangxi University, Nanning, China.

His research interests include power quality and power electronic transformer.

Ziguang Lu received the B.S. and M.S. degrees in electrical engineering from the University of Science and Technology Beijing, Beijing, China, in 1985 and 1988, respectively, and the Ph.D. degree in electric machines from Tsinghua University, Beijing, in 2004.

He became an Associate Professor in 1991 and a Professor in 2004. He is currently a Professor with Guangxi University, Nanning, China. His research interests include power electronics application, optimized control technologies of induction machines and their applications in distributed power systems. He was in charge of more than ten valuable scientific research projects, which brought benefits to industry.